Hindawi Publishing Corporation
Journal of Nanomaterials
Volume 2015, Article ID 358063, 9 pages
http://dx.doi.org/10.1155/2015/358063

Research Article

Photovoltaic and Impedance Properties of Hierarchical TiO_2 Nanowire Based Quantum Dot Sensitized Solar Cell

Amanullah Fatehmulla, M. Aslam Manthrammel, W. A. Farooq, Syed Mansoor Ali, and M. Atif

Department of Physics and Astronomy, College of Sciences, King Saud University, P.O. Box 2455, Riyadh 11451, Saudi Arabia

Correspondence should be addressed to Amanullah Fatehmulla; aman@ksu.edu.sa

Received 21 January 2015; Revised 11 May 2015; Accepted 17 May 2015

Academic Editor: Ion Tiginyanu

Growth and characterization of TiO_2 nanowire (NW) assemblies on FTO glass using a typical hydrothermal synthesis have been reported. CdS quantum dots (QDs) have been deposited on TiO_2 nanowires by successive ion layer adsorption and reaction (SILAR) method. FESEM image exhibits the flower-like hierarchical TiO_2 bunch of nanowires. HRTEM image confirms the size of CdS QDs between 5 and 6 nm. XRD and absorption studies revealed proper growth of CdS quantum dots on TiO_2 nanowires. At AM 1.5 illumination intensity, the solar cell, with the configuration FTO/TiO_2-NW/CdS-QDs/Pt-FTO, displays a short circuit current (J_{sc}) of 1.295 mA and an open circuit voltage (V_{oc}) of 0.38 V. The V_{oc} and J_{sc} showed linear behavior at higher illumination intensities. The peak in power-voltage characteristics at various illuminations showed a shift towards higher V_{oc} values. Capacitance-voltage (C-V), conductance-voltage (G-V), and series resistance-voltage (R_s-V) measurements of the cell in the frequency ranging from 5 kHz to 5 MHz showed decreasing trend of capacitance with increase of frequency whereas increase in conductance and decrease in resistance have been noticed with increase of frequency. All the results including the individual behavior of the plots of capacitance, conductance, and series resistance as a function of bias voltage have been discussed.

1. Introduction

To address the current energy crisis and remedy to the pollution from conventional energy resources, the unlimited solar energy provides us a solution for an economically feasible and clean source of energy. In the recent past, for the improvement of solar cells, substantial emphasis on research has been devoted towards the application of quantum dots (QDs), also known as semiconductor nanocrystals (NCs), because of their interesting optoelectronic properties [1–6]. QDs find interesting applications as their band gap can easily be tailored by adjusting their size to suit the solar spectrum [7, 8]. High extinction coefficients and large intrinsic dipole moments of QDs contribute to speedy charge separation [9]. Besides, QDs offer novel prospects to create hot electrons and multiple electron-hole pairs with a distinct photon via impact ionization [10, 11]. Due to these exciting features, relatively narrow band gap semiconductor QDs are found to be perfect candidates towards the optimization of solar cell to obtain enhanced performance. A distinctive approach to fabricate quantum dots sensitized solar cells (QDSSCs) is to choose semiconductor QDs as light absorbing candidates to sensitize wide band gap metal oxide nanostructured films such as SnO_2 [12], ZnO [13], and TiO_2 [14, 15]. Quantum dots (QDs) from inorganic semiconductors such as CdS [16], CdSe [17], CdTe [18], PbS [19], and Bi_2S_3 [20], which absorb light in the visible region, have been discovered to assist as sensitizers in place of dye molecules for photovoltaic cells. CdS, with broadly tunable band gap, is considered to be one of the potential photovoltaic materials. The sensitization of wide band gap semiconductors such as TiO_2 by the QDs is a strategic configuration for collecting the visible light used in photoelectrochemical applications.

One-dimensional nanostructures that include wires, rods, belts, and tubes have demonstrated increasing interest due to their attractive properties and exceptional uses [21]. As

compared to other low dimensional systems, the distinctive feature of nanowires is that they possess two quantum confined directions while still leaving one unconfined direction for electrical conduction. Hence, they find application where electrical conduction rather than tunneling is required [22, 23].

Titanium oxide exists in three crystallographic forms known as anatase, rutile, and brookite. Extensive studies have been carried out on one-dimensional (1D) anatase TiO_2 nanostructures such as nanotubes, nanorods [24], nanofibers, and nanowires [25], which offer better 1D electron transport path during the solar energy conversion process. The challenging task of increasing the current energy conversion efficiency of a solar cell is modification of 1D TiO_2 structure at the nanoregime. It is anticipated that split nanostructures can result in enlarged specific surface area and improved electron conductivity for enhanced photocurrent harvest efficiency [26]. Several reports exist on branched nanostructures synthesized by vapor or wet chemical methods [27, 28], but reports on the synthesis of 1D TiO_2 flower-like hierarchical hyperbranched nanostructures (aggregates of nanowires) and their sensitized composite structures are fewer.

In the present work, QDSSC is fabricated using flower-like hierarchical TiO_2 hyperbranched nanostructure (clusters of nanowires) which was synthesized through hydrothermal process. CdS QDs are acquired by successive ion layer adsorption and reaction (SILAR) method in order to sensitize TiO_2 hyperbranched nanowires based microspheres films for the solar cell. Morphological, structural, and optical characterizations have been carried out and finally the photovoltaic and impedance properties of the solar cell with the configuration FTO/TiO_2-NW/CdS-QD/Pt-FTO have been discussed.

2. Experimental Details

2.1. Synthesis of TiO_2 Nanowires. Flower-like hierarchical TiO_2 nanowire assemblies were grown on FTO substrates. In a typical synthesis, the substrate was ultrasonically cleaned sequentially in acetone, isopropyl alcohol (IPA), and deionized (DI) water for 15 min each and was finally dried under N_2 flow. Separately, 1 mL of a titanium isopropoxide solution was added dropwise to a 1 : 1 mixture of DI water and concentrated (35%) hydrochloric acid to obtain a clear transparent solution. The substrate was placed at an angle in a 60 mL Teflon liner and the precursor solution was added to it. The Teflon liner was loaded in an autoclave and was placed in an oven at 150°C for 15 hrs. After synthesis, the autoclave was cooled to room temperature and the substrates were taken out, rinsed extensively with deionized water, and left to dry in ambient air. TiO_2 coated substrates were finally treated with diluted $TiCl_4$ solution at 60°C, for 15 min.

2.2. Synthesis of CdS Quantum Dots. The quantum dots are deposited on TiO_2 coated FTO film by SILAR technique. This film was dipped into a 0.2 M cadmium nitrate ($Cd(NO_3)_2$) ethanol solution (cadmium cationic precursor) for 5 min, rinsed with ethanol, heated for 5 min, cooled to room temperature, and then dipped for another 5 min into a 0.2 M sodium sulfide (Na_2S) water solution (sulphur anionic precursor) and rinsed again with water, heated for 5 min, and cooled to room temperature. The CdS adsorbed TiO_2 film is dried with N_2 air stream. The two-step dipping procedure is called one SILAR cycle and the process was repeated for 6 cycles.

2.3. Preparation of Electrolyte Solution. Polysulfide electrolytes were prepared by mixing suitable quantities of Na_2S, S, and KCl powders in water/methanol solution taken in the ratio 3/7.

2.4. Fabrication of QDSSC Cell. The QD-adsorbed TiO_2 film was used as the working electrode and platinum coated FTO glass as counter electrode. The electrodes were assembled into a sealed cell with a cellotape spacer and binder clips with an active area equal to the area of 0.28 cm^2. A suitable electrolyte solution was introduced to this sealed cell. The electrolyte was injected from the edges into the open cell, and the cell was tested immediately.

2.5. Characterization Details. XRD analysis was done on TiO_2/FTO films using multipurpose X-ray diffractometer (Bruker, D8 Discover) with Cukα source radiation. Surface morphology of the films was carried out by using JEOL (JSM-7600F) Field Emission Electron Microscope (FESEM) as well as JEOL-2100F Transmission Electron Microscope (HRTEM). Optical absorption studies were made at room temperature by using UV-Vis-NIR Spectrophotometer (JASCO V-670) in the wavelength range of 200–800 nm. The current-voltage and capacitance-voltage characteristics were investigated using a Semiconductor Characterization System SC-4200 from Keithley. The films were illuminated by a Class-BBA Solar Simulator and TM-206 Solar Power Meter was used for measurement of light intensity.

3. Results and Discussion

3.1. Morphological Studies of the As-Prepared TiO_2 Nanowire Clusters and CdS QDs. Figure 1(a) shows FESEM image of a hierarchical structure which is flower-like clusters of TiO_2 nanowires on FTO substrate. The average diameter of the nanowire was 25 nm, exhibiting directly aligned one-dimensional nanostructure on the FTO substrate. This image approves the growth of a nanowire structure. This TiO_2 architecture may extend a one-dimensional electron pathway of photo injected electrons along the photoanode, and such a design would be more expedient to overpower the charge recombination between the photo injected electron in the photoanode and the cation in the electrolyte [29, 30].

The surface morphology of the SILAR grown CdS QDs on TiO_2 nanowire clusters studied by the high resolution transmission electron microscopy (HRTEM) is shown in Figure 1(b). The existence of lattice planes is evident in the HRTEM image which indicates the crystallinity in CdS quantum dots [31]. The image also depicts substantial dispersion of CdS QDs and most of the dots are observed to have the elliptical profile with diameter ranging from 5 to 6 nm. Two encircled quantum dots with clear lattice planes can be seen in the figure.

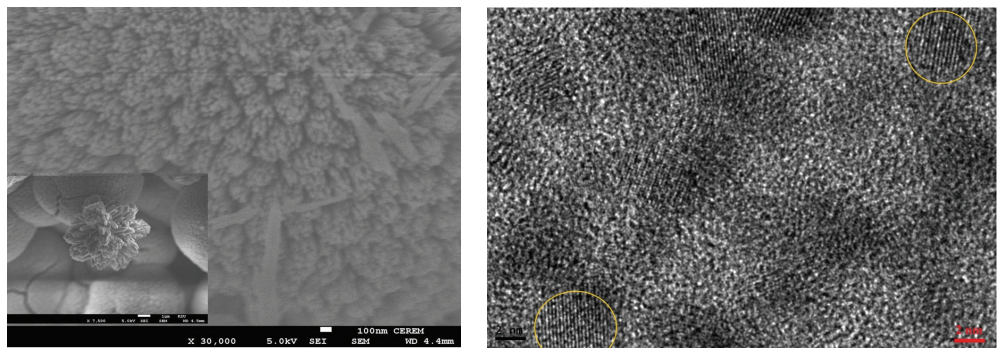

(a) (b)

FIGURE 1: (a) FESEM image of flower-like clusters of TiO_2 nanowires on FTO substrate (inset: lower magnification image). (b) HRTEM image of CdS QDs embedded on TiO_2NWs.

3.2. XRD Analysis of the As-Prepared TiO_2 Nanowire Clusters and CdS QDs Embedded on TiO_2 Nanowire Clusters. Typical XRD pattern of the as-prepared TiO_2 nanowire clusters sample is shown in Figure 2(a). XRD shows that the film on fluorine doped tin oxide (FTO) substrate has been indexed to rutile phase of TiO_2. The diffraction peaks are relatively sharp and agree well with those of the tetragonal TiO_2 with rutile structure (JCPDS 01-076-0318) [32] while Figure 2(a) also exhibits the characteristic peaks indexed to FTO (highlighted with stars) and similar observations are reported by Lee and Lu [33] as well. All the diffraction peaks also agree well with those of tetragonal TiO_2 with rutile structure in Crystallography Open Database (COD number 96-900-9084, P/42 *m n m*, $a = b = 0.45937$ nm, and $c = 0.29581$ nm) [34]. The average crystallite size of the TiO_2 nanowires was also calculated by Scherer's formula given by

$$D = \frac{0.9\lambda}{\beta \operatorname{Cos} \theta}, \quad (1)$$

where λ is the X-ray wavelength and β is the full width at half maximum by using the (110) diffraction peak at $2\theta = 27.43$ and was about 20–25 nm. The rutile phases match very well with the reports by Wyckoff [34], Baur and Khan [35], and Meagher and Lager [36].

Figure 2(b) shows the XRD pattern of TiO_2 nanowire clusters + CdS QDs embedded on TiO_2 nanowire clusters. The diffraction peaks (002), (101), (102), (110), (103), (112), (004), (211), (105), and (204) correspond to hexagonal (Wurtzite) CdS structure and agree very well with the JCPDS file # 00-006-0314. The XRD pattern in Figure 2(b) also depicts two characteristic peaks τ (002), (0–2 1) and A (101) which are indexed to Sn_2O_3 (JCPDS file # 00-020-1293) and anatase phase of TiO_2 (JCPDS file # 01-071-1166), respectively. The two characteristic peaks +(040) and +(322) are indexed to $Cd(NO_3)$ (JCPDS file # 01-070-0155) which signify the traces of precursor used for Cd source. However, by and large, the XRD pattern illustrates the characteristic peak alignments of TiO_2 and CdS, indicating the implantation of CdS QDs into the TiO_2 matrix [37].

3.3. Absorption Studies. Figure 3 shows the UV-Vis optical absorption spectra of as-prepared TiO_2 nanowire clusters and

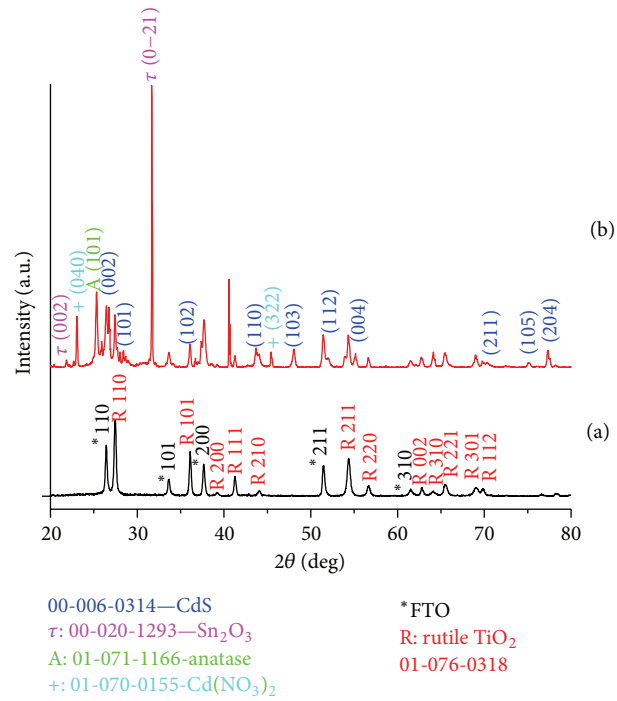

FIGURE 2: (a) XRD pattern of TiO_2 nanowire clusters on FTO. (b) XRD pattern of CdS QD embedded on TiO_2 nanowire clusters.

CdS QDs coated on TiO_2 nanowire clusters with different SILAR cycles 0, 2, 4, and 6. Figure 3 exhibits the fact that TiO_2 nanowire clusters film largely absorbs UV light, having an absorption band at 370 nm; this can be attributed to the wide band gap of rutile (3.35 eV) which is greater than the bulk rutile (3.0 eV) [38]. It can be seen that with SILAR cycles 2 and 4 CdS-QDs sensitization, CdS-QDs/TiO_2-NWs film exhibits marginal red shifted absorption. However, with SILAR cycle 6 CdS-QDs sensitization, the CdS-QDs/TiO_2-NWs film shows significant red shifted absorption band at 422 nm (2.94 eV) in the visible region which enables the absorption of ample visible light with increased intensity. The calculated band gaps are higher than the bulk CdS (2.38 eV) indicating that the size of the CdS coated on the TiO_2 nanowire clusters film is within the scale of QDs [39]. Therefore, it is established that TiO_2

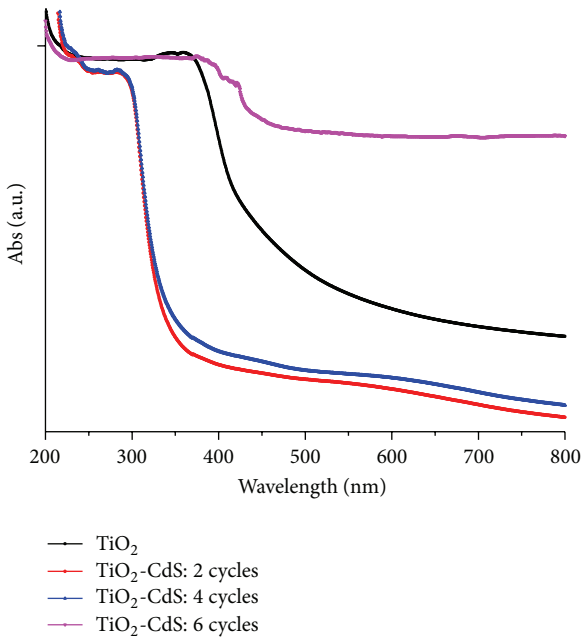

Figure 3: UV-Vis absorption spectra of CdS: TiO_2 NWs with different SILAR cycles 0, 2, 4, and 6.

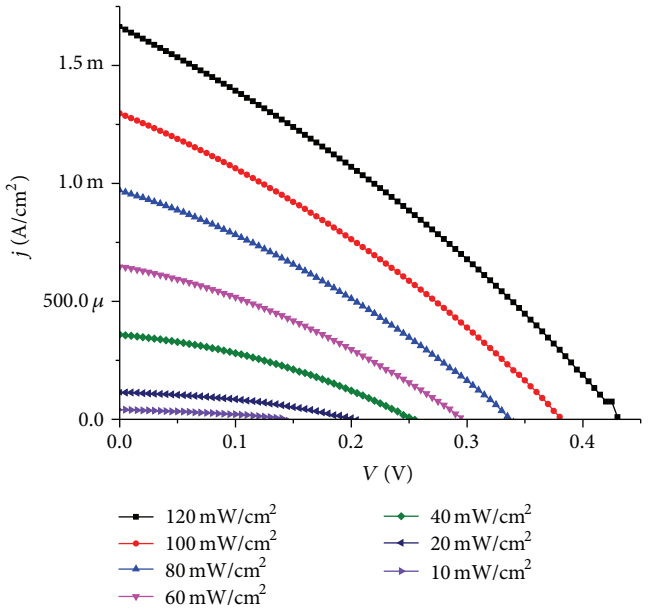

Figure 4: Current-voltage characteristics of FTO/TiO_2-NW/CdS-QD/Pt-FTO solar cell.

nanowire clusters film sensitized with CdS nanocrystals takes the lead for harvesting the visible light.

Furthermore, from the UV-Vis analysis and taking into account the absorption edge at 422 nm, the QDs radius was estimated by using the hyperbolic band model (HBM) given by [40]

$$R = \sqrt{\frac{2\pi^2\hbar^2 E_{\text{bulk}}}{m^*\left(E_{\text{nano}}^2 - E_{\text{bulk}}^2\right)}}, \quad (2)$$

where E_{bulk} denotes bulk band gap, E_{nano} stands for band gap of nanomaterial, and m^* is effective mass of electron in bulk CdS ($m^* = 0.19m_e$). The calculated QDs radius was found to be 2.52 nm. Therefore, the particle size was evaluated as twice the radius; that is, $2R = 5.04$ nm.

3.4. Photovoltaic Properties. CdS-QDs sensitized TiO_2 nanowires photoelectrode was fabricated to study the photoelectrochemical properties in solar cells. For a solar cell, the open circuit voltage is given by [41–43]

$$V_{\text{oc}} = \frac{nkT}{q} \ln\left(\frac{J_{\text{sc}}}{J_o} + 1\right), \quad (3)$$

where n is the diode ideality factor, k is Boltzmann's constant, q is the electric charge, and J_o is the reverse saturation current density. The photocurrent-voltage (I-V) characteristics of the solar cell with the configuration FTO/TiO_2-NW/CdS-QD/Pt-FTO are shown in Figure 4. It is evident that the photocurrent and photovoltage values exhibit increasing behavior with increasing illumination intensities. We observe an enhanced current density values which match well with the previous reports of increase in electrical conduction by the use of QDs [44, 45].

The cell measured a short circuit current (J_{sc}) of 1.295 mA/cm^2 and an open circuit voltage (V_{oc}) of 0.38 V at AM 1.5 illumination intensity.

The plot of short circuit current density J_{sc} versus open circuit voltage V_{oc} is illustrated in Figure 5(a). Increase of J_{sc} increases the value of V_{oc} exponentially. This exponential behavior of V_{oc} with J_{sc} obeys the relationship given in (3) [42, 43]. By using (3), the graph of V_{oc}-J_{sc} is fitted to determine the ideality factor and is found to be 3 [46]. Under room temperature, the ideality factor is considered to be approximately 1 for an ideal p-n junction diode. The possible explanations for higher ideality factors may be due to various imperfections and also due to local nonlinear shunts anywhere in the cell area that are accountable for the ideality factor value larger than 1 [47]. The value of short circuit current density J_{sc} of the solar cell can be determined using J-V curves under light illumination. In Figure 5(b), it can be seen that there exists a nonlinear relationship between current and light intensity in the low intensity region. This occurs due to the large shunt resistance in the device. The linear relation is completely restored after the light intensity is increased to 40 mW/cm^2 which indicates that the photofilling effect has saturated the nonradiative recombination center.

PV measurements at various intensities provide better understanding to the photoconduction performance as well as photosensing aspects of the cell. Figure 6 shows the plot of electric power versus voltage for FTO/TiO_2-NW/CdS-QD/Pt-FTO cell. The electric power increases with increasing of the bias voltage and reaches its maximum power and then decreases till it reaches zero value with the further increase of applied voltage. The maximum power is expressed as follows:

$$P_{\text{max}} = I_m \times V_m, \quad (4)$$

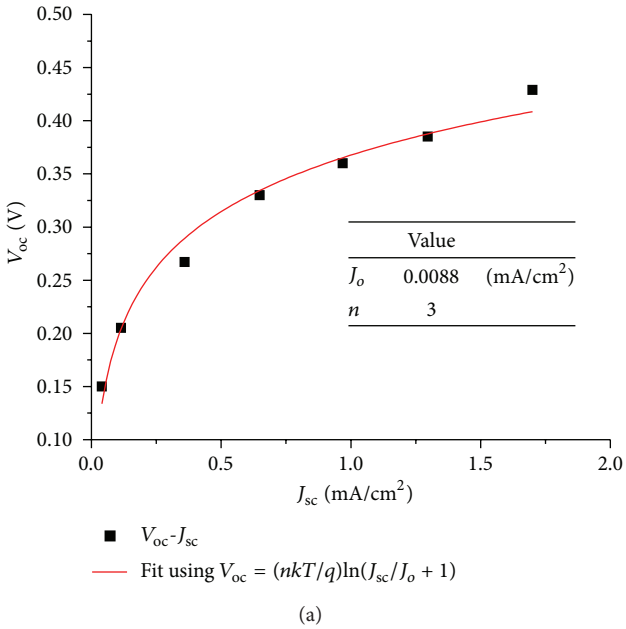

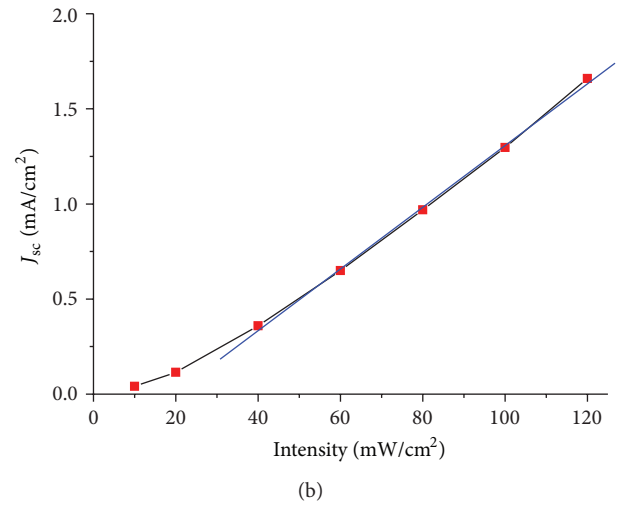

Figure 5: Photovoltaic performance parameter of FTO/TiO_2-NW/CdS-QD/Pt-FTO solar cell. (a) V_{oc}-J_{sc}; (b) J_{sc}-light intensity.

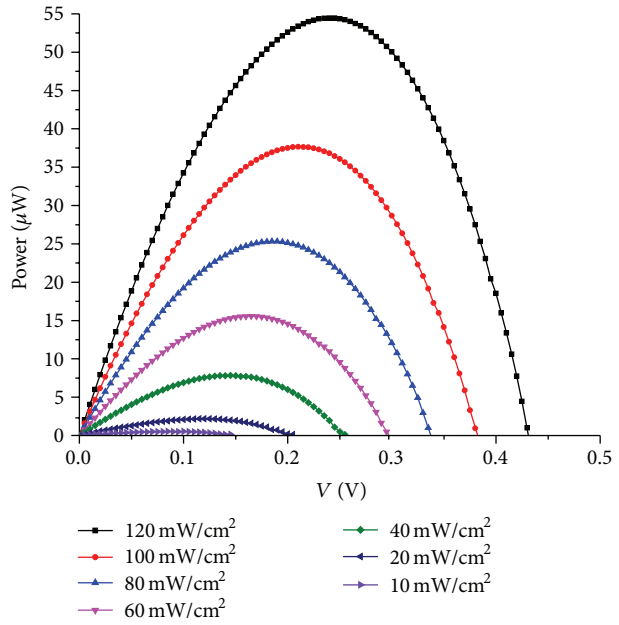

Figure 6: Power-voltage characteristics of FTO/TiO_2-NW/CdS-QD/Pt-FTO solar cell.

where I_m and V_m stand for the maximum current and maximum voltage, respectively, at each illumination intensity. The maximum power value designates how much the QDSSC can supply its maximum power to an external load. From Figure 6, it can also be seen that the maximum power point is moved to the higher voltages with the increasing incident light as follows: 0.14 V, 2 μW at 20 mW/cm^2 and 0.25 V, 54.3 μW at 120 mW/cm^2, respectively.

3.5. Impedance Properties

3.5.1. Capacitance-Voltage Characteristics. Figure 7(a) displays the *C-V* characteristics at different frequencies (from 5 kHz to 5 MHz) for FTO/TiO_2-NW/CdS-QD/Pt-FTO solar cell. To know the cell capacitance profile or admittance spectroscopy of TiO_2-NW based CdS QDSSC, it is useful to study the capacitance-voltage characteristics in a widespread frequency range. The capacitance measured by impedance spectroscopy studies at the solid/electrolyte interface of the cell is actually the total capacitance obtained from the electronic states (C_μ), the space charge (C_{sc}) on the semiconductor side, Helmholtz layer (C_H), and the surface adsorbed ionic species (C_{ad}) on the electrolyte side, where C_μ, C_{sc}, C_H, and C_{ad} are in parallel with ($C_\mu|C_{sc}$–$C_H|C_{ad}$), respectively, as reported by Wang et al. [48]. Gerischer and Seraphin have designated this as a simple three-layer model [49, 50]. It is elaborated by them to differentiate within the electric double layer: (i) the space charge region in the electrolyte (also known as Gouy layer (C_G) or diffused part of the ionic layer) with thickness of 1–10 nm, (ii) an intermediate region called Helmholtz layer (C_H) with thickness of 0.4–0.6 nm, and (iii) the space charge layer in the semiconductor (C_{sc}) with thickness of 10–100 nm. These capacitances add to the total capacitance of the interface in a way and they are in series $1/C = 1/C_{sc} + 1/C_H + 1/C_G$. Since S_H and S_G are very small because of the lower thickness of the Gouy and Helmholtz layers, their contribution to the total capacitance is negligible and hence neglected. It can be viewed that, with the increase of bias voltage from −2.0 V to +2.0 V, the capacitance also shows an intermittent increasing trend and thereafter it reaches a maximum followed by a decrease in its values, showing an increasing behavior after the bias voltage 1.3 V for 5 kHz and 10 kHz (almost similar stabilized behavior) frequencies. However, by increasing the frequency from 50 kHz to 5 MHz the device capacitance represents a decreasing trend towards zero. Figure 7(b) demonstrates the *C-V* characteristics at different higher frequency range from 500 kHz to 5 MHz showing a decreasing trend of capacitance values leading to zero. Here, at each frequency the overall behavior of capacitance seems to be almost saturated with the

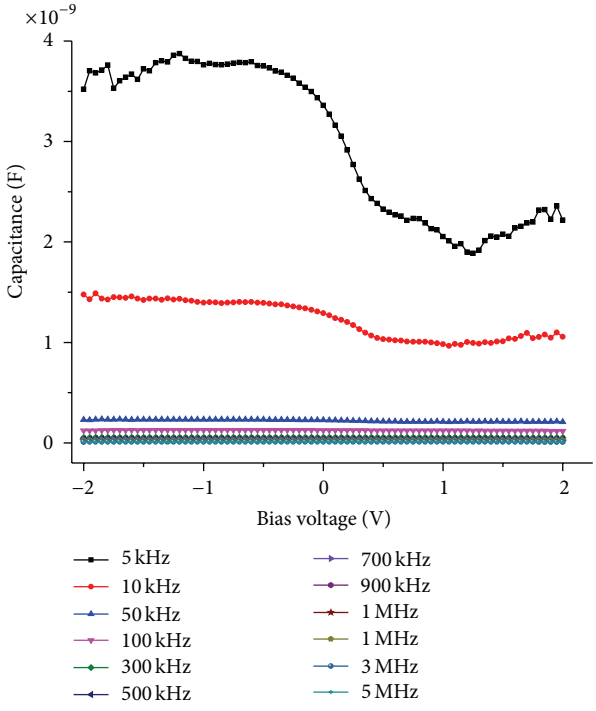

(a)

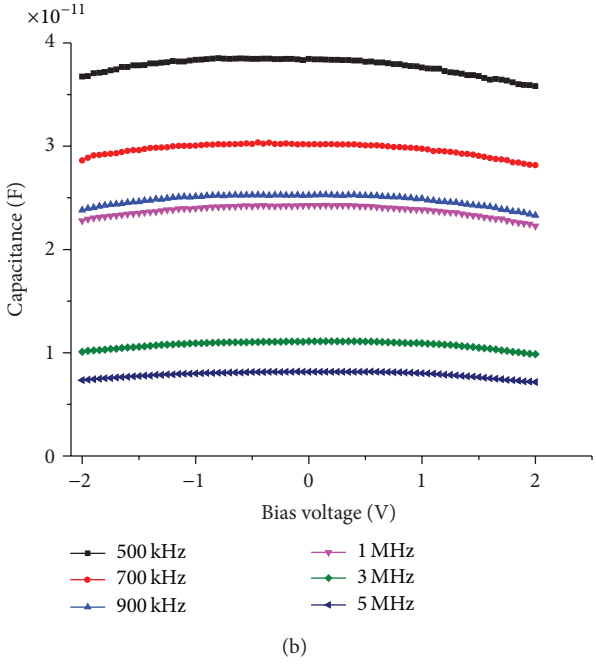

(b)

Figure 7: *C-V* characteristics of FTO/TiO_2-NW/CdS-QD/Pt-FTO solar cell: (a) at 5 kHz to 5 MHz frequency range and (b) at higher frequencies.

increase of bias voltage from −2 V to +2 V. However, from each of the plots, it can be seen that a marginal increase of capacitance is noticed with the increase of bias voltage from −2 V to −1 V, saturated in the bias range from −1 V to +1 V, and thereafter shows a minimal decrease in the bias range from +1 to +2 V. The plot exhibits neither a severe fall nor a negative capacitance trend in the whole range from

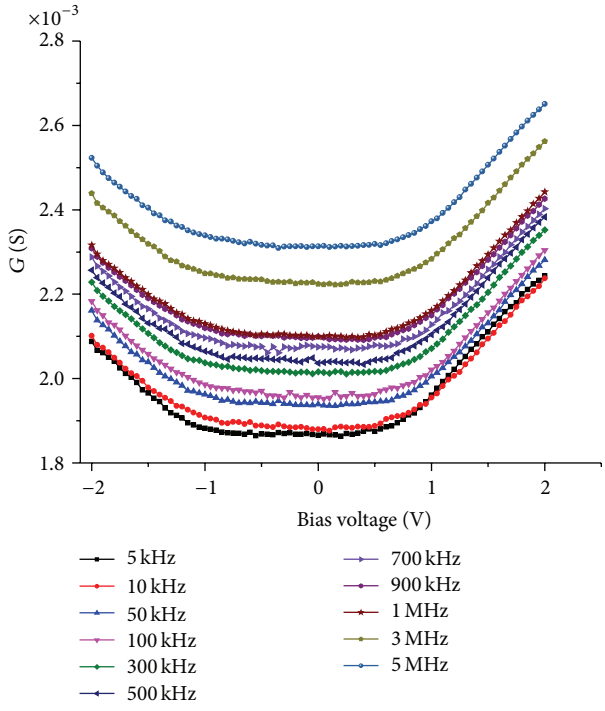

Figure 8: *G-V* characteristics of FTO/TiO_2-NW/CdS-QD/Pt-FTO solar cell at different frequencies.

−2 V to +2 V and even at higher frequencies as described by most of the impedance spectroscopy reports with DSSCs or QDSSCs [51, 52]. The basis of negative capacitance is usually ascribed to the injection of electron from front FTO electrode into TiO_2 [51]. The nonexistence of negative capacitance in this range for these types of films could possibly be due to the surface alteration of the FTO layer for the formation of the hierarchical structure of TiO_2 as elucidated in the morphological section earlier.

3.5.2. Conductance-Voltage Characteristics (G-V). Figure 8 shows the room temperature measured plots of conductance as a function of bias voltage from −2 V to +2 V for FTO/TiO_2-NW/CdS-QD/Pt-FTO solar cell at different frequencies. This is an established technique on the losses of conductance because of the exchange of majority carriers between the interface states and majority carrier band of the semiconductor when a small ac signal is applied (25 mV in the present study) to the semiconductor devices [53]. It is evident from Figure 8 that the conductance decreases and reaches a minimum of around −1.0 bias voltage and thereafter shows a saturation trend up to +1.0 V and then shows an increasing behavior up to the bias voltage +2 V. Furthermore, there is a gradual increase in conductance values with the increase of applied frequency from 5 kHz to 1 MHz. However, there is a noticeable increase in its values with the frequency increase of 3 MHz and 5 MHz.

3.5.3. Series Resistance-Voltage Characteristics (R_s-V). For a device, the noise ratio in terms of frequency can be determined using significant parameter known as series resistance

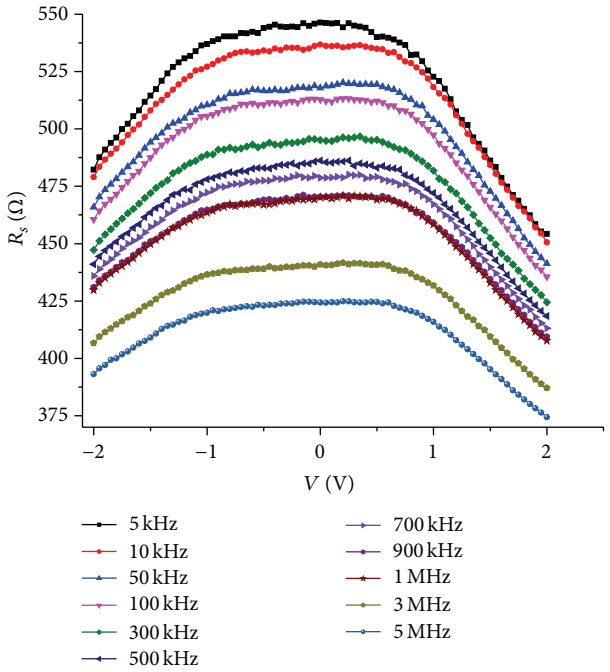

FIGURE 9: R_s-V characteristics of FTO/TiO_2-NW/CdS-QD/Pt-FTO solar cell at different frequencies.

R_s [54]. Hence, it is important to evaluate the values of R_s at different voltages in a wide frequency range. From the investigated *C-V-f* measurements, the voltage and frequency dependent series resistance of the device can be evaluated as [55]

$$R_s = \left(\frac{G_{MA}}{G_{MA}^2 + \omega^2 C_{MA}^2} \right), \quad (5)$$

where G_{MA} and C_{MA} denote the measured values of conductance and capacitance, respectively. Figure 9 shows the R_s-V characteristics of FTO/TiO_2-NW/CdS-QD/Pt-FTO solar cell at different frequencies. It can be seen from Figure 9 that the series resistance increases and reaches a maximum of around −1.0 bias voltage and thereafter shows a saturation trend around +1.0 V and then shows a decreasing behavior up to the bias voltage +2.0 V. Furthermore, there is a gradual decrease in resistance values with the increase of applied frequency from 1 MHz. However, there is noticeable decrease in its values with the increase of 3 MHz and 5 MHz frequencies. This is interpreted as follows. At low frequencies, the interface states can track the ac signal and harvest an excess capacitance which depends on the frequency [56]. At higher frequencies, the interface states cannot track the ac signal. In this situation, the input of interface state capacitance to the total capacitance is very minimal.

4. Conclusions

We have successfully synthesized flower-like hierarchical TiO_2 nanowire clusters on FTO substrates. CdS QDs were deposited on these nanowire clusters using SILAR technique. FESEM image revealed that the average diameter of the nanowire was 25 nm. HRTEM image confirmed the size of CdS QDs in the range of 5-6 nm. XRD analysis, HRTEM, and UV-Vis absorption studies corroborated the effective implantation of CdS QDs into the TiO_2 matrix. The size of the CdS QDs was computed by HBM and found to be 5.04 nm. The fabricated solar cell with the configuration FTO/TiO_2-NW/CdS-QD/Pt-FTO measured a J_{sc} of 1.295 mA/cm^2 and V_{oc} of 0.38 V at AM 1.5 light intensity. The maximum power value of the device moved to the higher voltages with increasing incident light as follows: 0.14 V, 2 μW at 20 mW/cm^2 and 0.25 V, 54.3 μW at 120 mW/cm^2, respectively. Impedance spectroscopic investigation of the cell with *C-V*, *G-V*, and R_s-V plots exhibited frequency dependence which was varied between 5 kHz and 5 MHz in the bias voltage range from −2 V to +2 V. Capacitance showed decreasing trend with the increase of frequency whereas increase in conductance and decrease in series resistance with the increase in frequency have been recorded. The nonexistence of negative capacitance for these types of films could possibly be due to the surface alteration of the FTO layer for the formation of the hierarchical structure of TiO_2.

Conflict of Interests

The authors declare that there is no conflict of interests regarding the publication of this paper.

Acknowledgment

This project was funded by the National Plan for Science, Technology and Innovation (MAARIFAH), King Abdulaziz City for Science and Technology, Kingdom of Saudi Arabia, Award no. 11NAN 1464-02.

References

[1] S. Emin, S. P. Singh, L. Han, N. Satoh, and A. Islam, "Colloidal quantum dot solar cells," *Solar Energy*, vol. 85, no. 6, pp. 1264–1282, 2011.

[2] E. M. Barea, M. Shalom, S. Giménez et al., "Design of injection and recombination in quantum dot sensitized solar cells," *Journal of the American Chemical Society*, vol. 132, no. 19, pp. 6834–6839, 2010.

[3] M. Shalom, S. Buhbut, S. Tirosh, and A. Zaban, "Design rules for high-efficiency quantum-dot-sensitized solar cells: a multilayer approach," *The Journal of Physical Chemistry Letters*, vol. 3, no. 17, pp. 2436–2441, 2012.

[4] Y. Bu, Z. Chen, W. Li, and J. Yu, "High-efficiency photoelectrochemical properties by a highly crystalline CdS-sensitized ZnO nanorod array," *ACS Applied Materials and Interfaces*, vol. 5, no. 11, pp. 5097–5104, 2013.

[5] J.-G. Song, X. Song, T. Ling, X.-W. Du, and S. Z. Qiao, "Enhancing the conversion efficiency of semiconductor sensitized solar cells via the cosensitization of dual-sized quantum dots," *Industrial & Engineering Chemistry Research*, vol. 51, no. 30, pp. 10074–10078, 2012.

[6] V. González-Pedro, Q. Shen, V. Jovanovski et al., "Ultrafast characterization of the electron injection from CdSe quantum

dots and dye N719 co-sensitizers into TiO_2 using sulfide based ionic liquid for enhanced long term stability," *Electrochimica Acta*, vol. 100, pp. 35–43, 2013.

[7] P. V. Kamat, "Quantum dot solar cells. Semiconductor nanocrystals as light harvesters," *The Journal of Physical Chemistry C*, vol. 112, no. 48, pp. 18737–18753, 2008.

[8] N. Balis, V. Dracopoulos, K. Bourikas, and P. Lianos, "Quantum dot sensitized solar cells based on an optimized combination of ZnS, CdS and CdSe with CoS and CuS counter electrodes," *Electrochimica Acta*, vol. 91, pp. 246–252, 2013.

[9] A. Kongkanand, K. Tvrdy, K. Takechi, M. Kuno, and P. V. Kamat, "Quantum dot solar cells. Tuning photoresponse through size and shape control of CdSe–TiO_2 architecture," *Journal of the American Chemical Society*, vol. 130, no. 12, pp. 4007–4015, 2008.

[10] M. C. Beard, J. M. Luther, O. E. Semonin, and A. J. Nozik, "Third generation photovoltaics based on multiple exciton generation in quantum confined semiconductors," *Accounts of Chemical Research*, vol. 46, no. 6, pp. 1252–1260, 2013.

[11] O. E. Semonin, J. M. Luther, S. Choi et al., "Peak external photocurrent quantum efficiency exceeding 100% via MEG in a quantum dot solar cell," *Science*, vol. 334, no. 6062, pp. 1530–1533, 2011.

[12] M. A. Hossain, J. R. Jennings, Z. Y. Koh, and Q. Wang, "Carrier generation and collection in CdS/CdSe-sensitized SnO2 Solar cells exhibiting unprecedented photocurrent densities," *ACS Nano*, vol. 5, no. 4, pp. 3172–3181, 2011.

[13] H. Kim, H. Jeong, T. K. An, C. E. Park, and K. Yong, "Hybrid-type quantum-dot cosensitized ZnO nanowire solar cell with enhanced visible-light harvesting," *ACS Applied Materials and Interfaces*, vol. 5, no. 2, pp. 268–275, 2013.

[14] P. V. Kamat, "TiO_2 nanostructures: recent physical chemistry advances," *Journal of Physical Chemistry C*, vol. 116, no. 22, pp. 11849–11851, 2012.

[15] X. Song, M. Wang, J. Deng et al., "One-step preparation and assembly of aqueous colloidal CdS_xSe_{1-x} nanocrystals within mesoporous TiO_2 films for quantum dot-sensitized solar cells," *ACS Applied Materials & Interfaces*, vol. 5, no. 11, pp. 5139–5148, 2013.

[16] X.-F. Gao, W.-T. Sun, Z.-D. Hu et al., "An efficient method to form heterojunction CdS/TiO_2 photoelectrodes using highly ordered TiO_2 nanotube array films," *Journal of Physical Chemistry C*, vol. 113, no. 47, pp. 20481–20485, 2009.

[17] L. W. Chong, H. T. Chien, and Y. L. Lee, "Assembly of CdSe onto mesoporous TiO_2 films induced by a self-assembled monolayer for quantum dot-sensitized solar cell applications," *Journal of Power Sources*, vol. 195, no. 15, pp. 5109–5113, 2010.

[18] Y. W. Tang, X. Y. Hua, M. J. Chen, L. J. Luo, B. H. Li, and L. Z. Zhang, "CdSe nanocrystal sensitized ZnO core-shell nanorod array films: preparation and photovoltaic properties," *Electrochimica Acta*, vol. 54, no. 10, pp. 2742–2747, 2009.

[19] A. Kumar and A. Jakhmola, "RNA-mediated fluorescent Q-PbS nanoparticles," *Langmuir*, vol. 23, no. 6, pp. 2915–2918, 2007.

[20] R. Brahimi, Y. Bessekhouad, A. Bouguelia, and M. Trari, "Visible light induced hydrogen evolution over the heterosystem Bi_2S_3/TiO_2," *Catalysis Today*, vol. 122, no. 1-2, pp. 62–65, 2007.

[21] Z. L. Wang, Ed., *Nanowires and Nanobelts—Materials, Properties and Devices*, vol. 1-2, Kluwer Academic, Boston, Mass, USA, 2003.

[22] J. Hu, T. W. Odom, and C. M. Lieber, "Chemistry and physics in one dimension: synthesis and properties of nanowires and nanotubes," *Accounts of Chemical Research*, vol. 32, no. 5, pp. 435–445, 1999.

[23] K. S. Shankar and A. K. Raychaudhuri, "Fabrication of nanowires of multicomponent oxides: Review of recent advances," *Materials Science and Engineering C*, vol. 25, no. 5–8, pp. 738–751, 2005.

[24] L. Liu, J. Qian, B. Li et al., "Fabrication of rutile TiO_2 tapered nanotubes with rectangular cross-sections via anisotropic corrosion route," *Chemical Communications*, vol. 46, no. 14, pp. 2402–2404, 2010.

[25] Z.-Y. Yuan, W. Zhou, and B.-L. Su, "Hierarchical interlinked structure of titanium oxide nanofibers," *Chemical Communications*, no. 11, pp. 1202–1203, 2002.

[26] J. K. Oh, J. K. Lee, H. S. Kim, S. B. Han, and K. W. Park, "TiO_2 branched nanostructure electrodes synthesized by seeding method for dye-sensitized solar cells," *Chemistry of Materials*, vol. 22, no. 3, pp. 1114–1118, 2010.

[27] Y. Jung, D. K. Ko, and R. Agarwal, "Synthesis and structural characterization of single-crystalline branched nanowire heterostructures," *Nano Letters*, vol. 7, no. 2, pp. 264–268, 2007.

[28] T. L. Sounart, J. Liu, J. A. Voigt, M. Huo, E. D. Spoerke, and B. McKenzie, "Secondary nucleation and growth of ZnO," *Journal of the American Chemical Society*, vol. 129, no. 51, pp. 15786–15793, 2007.

[29] S. H. Kang, S.-H. Choi, M.-S. Kang et al., "Nanorod-based dye-sensitized solar cells with improved charge collection efficiency," *Advanced Materials*, vol. 20, pp. 54–58, 2008.

[30] K. Mukherjee, T.-H. Teng, R. Jose, and S. Ramakrishna, "Electron transport in electrospun TiO_2 nanofiber dye-sensitized solar cells," *Applied Physics Letters*, vol. 95, no. 1, Article ID 012101, 3 pages, 2009.

[31] H. Dhyani, C. Dhand, B. D. Malhotra, and P. Sen, "Polyaniline-CdS quantum dots composite for mediator free biosensing," *Journal of Biosensors and Bioelectronics*, vol. 3, article 112, 2011.

[32] J. Yi, Y. Liu, Y. Wang, X. Li, S. Hu, and W. Li, "Synthesis of dandelion-like TiO_2 microspheres as anode materials for lithium ion batteries with enhanced rate capacity and cyclic performances," *International Journal of Minerals, Metallurgy, and Materials*, vol. 19, no. 11, pp. 1058–1062, 2012.

[33] K.-T. Lee and S.-Y. Lu, "Porous FTO thin layers created with a facile one-step Sn^{4+}-based anodic deposition process and their potential applications in ion sensing," *Journal of Materials Chemistry*, vol. 22, no. 32, pp. 16259–16268, 2012.

[34] R. W. G. Wyckoff, *Crystal Structures*, vol. 1, Interscience Publishers, New York, NY, USA, 2nd edition, 1963.

[35] W. H. Baur and A. A. Khan, "Rutile-type compounds. IV. SiO_2, GeO_2 and a comparison with other rutile-type structures," *Acta Crystallographica Section B*, vol. 27, part 11, pp. 2133–2139, 1971.

[36] E. P. Meagher and G. A. Lager, "Polyhedral thermal expansion in the TiO_2 polymorphs; refinement of the crystal structures of rutile and brookite at high temperature," *Can Mineral*, vol. 17, no. 1, pp. 77–85, 1979.

[37] Q. Zhu, J. Chen, M. Xu et al., "Microsphere assembly of rutile TiO_2 hierarchically hyperbranched nanorods: CdS sensitization and photovoltaic properties," *Solid State Sciences*, vol. 13, no. 6, pp. 1299–1303, 2011.

[38] M. Xu, P. Da, H. Wu, D. Zhao, and G. Zheng, "Controlled Sn-doping in TiO_2 nanowire photoanodes with enhanced photoelectrochemical conversion," *Nano Letters*, vol. 12, no. 3, pp. 1503–1508, 2012.

[39] T. Nakanishi, B. Ohtani, and K. Uosaki, "Fabrication and characterization of CdS-nanoparticle mono- and multilayers on a self-assembled monolayer of alkanedithiols on gold," *Journal of Physical Chemistry B*, vol. 102, no. 9, pp. 1571–1577, 1998.

[40] S. S. Nath, M. Choudhury, G. Gope, and R. K. Nath, "PVA embedded ZnO quantum dots for methanol sens-ing," *NanoTrends*, vol. 8, pp. 1–4, 2010.

[41] M. L. Rosenblut and N. S. Lewis, "'Ideal' behavior of the open circuit voltage of semiconductor/liquid junctions," *The Journal of Physical Chemistry*, vol. 93, pp. 3735–3740, 1989.

[42] A. Hagfeldt, H. Lindström, S. Södergren, and S.-E. Lindquist, "Photoelectrochemical studies of colloidal TiO_2 films: the effect of oxygen studied by photocurrent transients," *Journal of Electroanalytical Chemistry*, vol. 381, no. 1-2, pp. 39–46, 1995.

[43] X. Sheng, Y. Zhao, J. Zhai, L. Jiang, and D. Zhu, "Electrohydrodynamic fabrication of ZnO-based dye sensitized solar cells," *Applied Physics A: Materials Science and Processing*, vol. 87, no. 4, pp. 715–719, 2007.

[44] P. T. Landsberg, H. Nussbaumer, and G. Willeke, "Band-band impact ionization and solar cell efficiency," *Journal of Applied Physics*, vol. 74, no. 2, pp. 1451–1452, 1993.

[45] A. J. Nozik, "Quantum dot solar cells," *Physica E*, vol. 14, no. 1-2, pp. 115–120, 2002.

[46] T. Sogabe, Y. Shoji, M. Ohba et al., "Intermediate-band dynamics of quantum dots solar cell in concentrator photovoltaic modules," *Scientific Reports*, vol. 4, article 4792, 2014.

[47] O. Breitenstein, M. Langenkamp, J. P. Rakotoniaina, and J. Zettner, "The imaging of shunts in solar cells by infrared lock-in thermography," in *Proceedings of the 17th European Photovoltaic Solar Energy Conference*, pp. 1499–1502, Munich, Germany, October 2001.

[48] Q. Wang, S. Ito, M. Grätzel et al., "Characteristics of high efficiency dye-sensitized solar cells," *The Journal of Physical Chemistry B*, vol. 110, no. 50, pp. 25210–25221, 2006.

[49] "Solid state physics," in *Solar Energy Conversion*, H. Gerischer and B. O. Seraphin, Eds., Springer, New York, NY, USA, 1979.

[50] M. Radecka, M. Rekas, A. Trenczek-Zajac, and K. Zakrzewska, "Importance of the band gap energy and flat band potential for application of modified TiO_2 photoanodes in water photolysis," *Journal of Power Sources*, vol. 181, no. 1, pp. 46–55, 2008.

[51] G. Kron, G. Nelles, T. Miteva, A. Yasuda, J. H. Werner, and U. Rau, "Junction Admittance of Dye Sensitized Nanoporous TiO_2 Solar Cells," http://www.electrochem.org/dl/ma/201/pdfs/1054.pdf.

[52] I. S. Yahia, H. S. Hafez, F. Yakuphanoglu, B. F. Senkal, and M. S. A. A. Mottaleb, "Photovoltaic and impedance spectroscopy analysis of p-n like junction for dye sensitized solar cell," *Synthetic Metals*, vol. 161, no. 13-14, pp. 1299–1305, 2011.

[53] E. H. Nicollian and A. Goetzberger, "Mos conductance technique for measuring surface state parameters," *Applied Physics Letters*, vol. 7, no. 8, pp. 216–219, 1965.

[54] S. A. Mansour and F. Yakuphanoglu, "Electrical-optical properties of nanofiber ZnO film grown by sol gel method and fabrication of ZnO/p-Si heterojunction," *Solid State Sciences*, vol. 14, no. 1, pp. 121–126, 2012.

[55] E. H. Nicollian and J. R. Brews, *MOS Physics and Technology*, John Wiley & Sons, New York, NY, USA, 1982.

[56] B. Akkal, Z. Benamara, B. Gruzza, and L. Bideux, "Characterization of interface states at Au/InSb/InP(100) Schottky barrier diodes as a function of frequency," *Vacuum*, vol. 57, no. 2, pp. 219–228, 2000.